New Journal of Physics
The open-access journal for physics

Loschmidt echo for the many-electron dynamics in nonparabolic quantum wells

G Manfredi[1,2] **and P-A Hervieux**[1]

[1] Institut de Physique et Chimie des Matériaux de Strasbourg, CNRS and Université Louis Pasteur BP 43, F-67034 Strasbourg, France
E-mail: Giovanni.Manfredi@ipcms.u-strasbg.fr

New Journal of Physics **11** (2009) 013050 (16pp)
Received 16 October 2008
Published 26 January 2009
Online at http://www.njp.org/
doi:10.1088/1367-2630/11/1/013050

Abstract. The Loschmidt echo (or quantum fidelity) is investigated in the context of the many-body electron dynamics in a nonparabolic quantum well, modeled by the self-consistent Wigner–Poisson system. The quantum fidelity drops abruptly after a quiescent period, as was observed for other self-interacting systems. A unifying interpretation of this phenomenon is given in terms of trajectory separation and the Ehrenfest time. The effects of Planck's constant and environment-induced decoherence are also studied.

Contents

[2] Author to whom any correspondence should be addressed.

1. Introduction

Small semiconductor devices, such as quantum dots and quantum wells, have been at the center of intense investigations, particularly for possible applications in the emerging field of quantum computing [1]. Compared to competing approaches [2] (ion traps, neutral atoms, superconducting circuits, etc), those based on solid-state devices have the advantage of relying on the long experience acquired on semiconductor microelectronics. To implement basic qubit operations, most proposed schemes make use of the electron spin states. Nevertheless, to manipulate the electrons themselves, it is still necessary to resort to electric fields, either static (dc) [3] or oscillating (laser pulses) [4]. For many-electron devices [5], it is therefore of paramount importance to understand the properties of the self-consistent electron dynamics and its stability with respect to external perturbations.

Several theoretical and computational studies have investigated the linear and nonlinear response of an electron gas confined in a quantum well, mainly using the time-dependent Hartree–Fock equations [6] or the density functional theory (DFT) [7]. The electron response strongly depends on the shape of the confining potential. For perfectly parabolic confinement, the response is dominated by the plasmon or the Kohn mode [8, 9], consisting of coherent oscillations of the electrons' center-of-mass at the plasma frequency. For nonparabolic confinement, the plasmon mode couples to the many degrees of freedom of the relative coordinate system. The latter acts as a thermal bath (i.e. an 'environment') on the center-of-mass coordinate, giving rise to dissipation and decoherence. This is an interesting situation since both the collective and the relative degrees of freedom stem from the same electron population, in contrast to the usual studies where the system and the environment are separate entities.

An interesting measure of the coherence of a quantum system is given by the Loschmidt echo, which describes the stability properties of the system under imperfect time reversal. An equivalent approach to the Loschmidt echo was proposed earlier by Peres [10] in terms of the so-called *quantum fidelity*. Peres noted that the stability of a quantum system against external perturbations can be measured by the overlap of two wavefunctions evolving in slightly different Hamiltonians. The quantum fidelity at time t is then defined as the square of the scalar product of the wavefunctions evolving in these Hamiltonians: $F(t) = |\langle\psi_1(t)|\psi_2(t)\rangle|^2$. Jalabert and Pastawski [11] have proven that for perturbations that are classically weak but quantum-mechanically strong, the fidelity decay rate only depends on the classical Lyapunov exponent of the unperturbed system. This universal behavior was later corroborated by numerical simulations [12, 13]. For weaker perturbations, the decay rate is still exponential, but perturbation-dependent (Fermi golden rule regime). For still weaker perturbations, the decay is Gaussian [12].

Most existing results are restricted to single-particle systems evolving in a given Hamiltonian. In two previous papers, we investigated the behavior of the quantum fidelity in a system of particles interacting via their mean field. In [14], we used a toy model based on fluid-like equations describing the self-consistent dynamics of a many-electron system. In [15], the Loschmidt echo scenario was applied to a system of interacting cold atoms forming a Bose–Einstein condensate. In the latter work, realistic physical parameters were used and an experiment was proposed to test the predictions of our model. For both systems, the numerical results showed that the quantum fidelity displays an anomalous behavior: it remains equal to unity until a critical time, then drops suddenly to much lower values. The critical time was found to depend logarithmically on the perturbation.

In the present paper, we study the Loschmidt echo for a system of electrons confined in a nonparabolic quantum well and interacting through their Coulomb mean field. The quantum electron dynamics is described by the Wigner equation, which can account for both pure and mixed quantum states. This is radically different from the previous results on the Loschmidt echo, which were mostly based on the Schrödinger representation and were thus restricted to pure states. In addition, the Wigner representation allows us to include the dissipative effects due, for instance, to disorder or phonon scattering. Again, this was not possible in previous simulations based on the Schrödinger equation, which were restricted to purely Hamiltonian (unitary) evolutions. Finally, instead of perturbing the Hamiltonian—as was the case for all previous studies—we perturb the initial condition. This is possible because of the nonlinear nature of the problem under study. In contrast, for the linear Schrödinger equation, the overlap of two wavefunctions evolving in the same Hamiltonian remains constant in time. Using the above tools, we can provide a unifying explanation for the anomalous fidelity decay in terms of trajectory separation in phase space. The critical time—at which the fidelity drops abruptly—emerges naturally as a kind of Ehrenfest time.

2. Model

To study the self-consistent electron dynamics, we make use of the Wigner representation of quantum mechanics. A mixed quantum state is represented by a function of the phase space variables plus time, $f(x, v, t)$ (we deal with one-dimensional problems), which evolves according to the Wigner equation

$$\frac{\partial f}{\partial t} + v\frac{\partial f}{\partial x} + \frac{im_*}{2\pi\hbar}\iint \mathrm{d}\lambda\,\mathrm{d}v' \mathrm{e}^{\mathrm{i}m_*(v-v')\lambda} f(x, v', t) \times \left[V\left(x + \frac{\lambda\hbar}{2}, t\right) - V\left(x - \frac{\lambda\hbar}{2}, t\right)\right] = \left(\frac{\partial f}{\partial t}\right)_{\text{scatt}}, \tag{1}$$

where m_* is the effective electron mass and $V(x, t)$ the total potential acting on the electrons. The latter is composed of two terms: the confining potential $V_{\text{conf}}(x)$ and the Hartree potential $V_{\text{H}}(x, t)$, which obeys the Poisson's equation

$$\frac{\partial^2 V_{\text{H}}}{\partial x^2} = \frac{e^2}{\varepsilon}\int_{-\infty}^{\infty} f\,\mathrm{d}v, \tag{2}$$

where e is the absolute electron charge and ε the effective dielectric constant. We consider wide quantum wells ($\approx$100 nm) at moderate electron temperatures, for which the exchange and correlation corrections can be neglected [16, 17]. The right-hand side of equation (1) models disorder or phonon scattering. Its exact form will be specified in section 3.

The confining potential is harmonic with a small quartic component:

$$V_{\text{conf}}(x) = \tfrac{1}{2}m_*\omega_0^2(x^2 + Kx^4). \tag{3}$$

As an initial condition, we take a Maxwell–Boltzmann distribution

$$f_0(x, v) = \frac{m_* n_{\text{e}}}{\sqrt{2\pi}\sigma_p}\exp\left(-\frac{(x - x_0)^2}{2\sigma_x^2} - \frac{{m_*}^2 v^2}{2\sigma_p^2}\right), \tag{4}$$

where n_{e} is the peak electron density, and the distribution is shifted by a distance x_0 to excite the dynamics. The variances σ_x and σ_p can be expressed in terms of the thermal speed

$v_{\rm th} = \sqrt{k_{\rm B} T_{\rm e}/m_*}$, where $T_{\rm e}$ is the electron temperature (supposed to be larger than the Fermi temperature $T_{\rm F}$). One has: $\sigma_x = v_{\rm th}/\omega_0$ and $\sigma_p = m_* v_{\rm th}$.

An important parameter is the so-called 'filling fraction', defined as $\eta = \omega_{\rm p}^2/\omega_0^2$, where $\omega_{\rm p} = (e^2 n_{\rm e}/m_* \varepsilon)^{1/2}$ is the electron plasma frequency. This parameter, which is proportional to the electron density, measures the relative importance of self-consistent effects (electrostatic repulsion) versus the strength of the confinement. Quantum effects are measured by the dimensionless Planck constant, $H = \hbar\omega_0/k_{\rm B} T_{\rm e} = \hbar/\sigma_x \sigma_{\rm p}$. To satisfy Heisenberg's uncertainty principle, one must have $H \leqslant 2$.

The quantum fidelity could be defined as follows:

$$F(t) = \frac{2\pi\hbar}{m_* N^2} \iint f_1(x, v, t) f_2(x, v, t)\, {\rm d}x\, {\rm d}v, \tag{5}$$

where $N = \iint f_{1,2}\, {\rm d}x\, {\rm d}v$ is the total number of electrons (which is the same for both evolutions). This definition reduces to the usual one for Schrödinger wavefunctions when f_1 and f_2 correspond to pure quantum states. However, for computational reasons, it is better to use a slightly different definition

$$F_W(t) = \frac{\iint f_1 f_2\, {\rm d}x\, {\rm d}v}{(\iint f_1^2\, {\rm d}x\, {\rm d}v)^{1/2} (\iint f_2^2\, {\rm d}x\, {\rm d}v)^{1/2}}. \tag{6}$$

Indeed, in a simulation of the Wigner equation, the quantity $\iint f^2\, {\rm d}x\, {\rm d}v$ slightly decreases because of numerical dissipation that entails loss of information at small scales [18]. Thus, the standard fidelity (equation (5)) could decrease simply because each quantity $\iint f_j^2\, {\rm d}x\, {\rm d}v$ ($j = 1, 2$) decreases as a result of numerical errors. The definition of equation (6) factors out these spurious effects, so that the fidelity is only affected by the difference between f_1 and f_2.

In the previous studies [14, 15], the fidelity decay arose because of a small perturbation of the Hamiltonian, while the initial conditions were exactly the same. This was in line with the original suggestion by Peres [10]. Indeed, for the linear Schrödinger equation, the overlap of two wavefunctions remains constant, if they evolve in the same Hamiltonian. However, for intrinsically nonlinear models like the one considered here, it should suffice to perturb the initial-quantum state (without doing anything to the Hamiltonian) to see some nontrivial decay of the corresponding fidelity. This is the approach that we adopt here.

The initial state, equation (4), is perturbed by shifting the Maxwellian distribution by a small amount δv_0 in velocity space. Both states then evolve in the same external potential. (It must be stressed that, since the Hartree potential depends self-consistently on the electron density, the Hamiltonians acting on each Wigner function will diverge with time.) The advantage of this approach is that the perturbation is characterized by a single number, i.e. the shift δv_0. As we shall see, the amplification of the initial perturbation in time is a crucial quantity to characterize the fidelity decay.

We use typical parameters for semiconductor quantum wells [7, 19]: effective electron mass and dielectric constant $m_\star = 0.067\, m_{\rm e}$ and $\varepsilon = 13\varepsilon_0$, respectively, oscillator energy $\hbar\omega_0 = 9.75\,{\rm meV}$ and oscillator length $L_{\rm ho} = \sqrt{\hbar/m_\star\omega_0} \simeq 11\,{\rm nm}$. For $\eta = 1$, this yields a maximum surface density $n_{\rm se} = 1.5 \times 10^{11}\,{\rm cm}^{-2}$, volume density $n_{\rm e} = 6 \times 10^{16}\,{\rm cm}^{-3}$, and Fermi temperature $T_{\rm F} = 96.8\,{\rm K}$. Thus, a temperature $T_{\rm e} \simeq 200\,{\rm K}$ corresponds to a normalized Planck constant $H \simeq 0.5$, whereas $T_{\rm e} \simeq 100\,{\rm K}$ corresponds to $H \simeq 1$.

The results were obtained with a numerical code based on a regular meshing of the two-dimensional phase space. The code combines the split-operator method with the fast Fourier

transforms in the velocity coordinate [20]. During the evolution, the Wigner function develops small-scale structures whose size is proportional to the effective Planck constant H. Therefore, a finer mesh is required in the semiclassical limit. Typically, we use $N_x = 2000$ and $N_v = 2048$ for $H = 1$, and $N_x = 8000$ and $N_v = 8192$ for $H = 0.1$. The time step is $\omega_0 \Delta t = 0.025$ for all cases.

3. Results

In this section, we present the numerical results issued from the solution of the Wigner–Poisson system (1) and (2). The dynamics is influenced by a relatively small number of parameters each of which determines the importance of a particular effect: (i) the filling fraction η (self-consistent effects), (ii) the parameter K in equation (3) and the initial shift x_0 (anharmonicity) and (iii) the reduced Planck constant H (quantum effects). We neglect for the moment dissipative effects.

To observe a nontrivial behavior of the quantum fidelity, the dynamics must be sufficiently complex (this had already been noticed in previous studies [14, 15]). As the confining potential is integrable, this means that self-consistent effects and thus the filling fraction η should be large. We have found that values $\eta \geqslant 5$ are generally sufficient. In addition, the anharmonic effects must also be significant. Indeed, for perfectly parabolic confinement, there is no interchange between the center-of-mass and the internal degrees of freedom of the electron gas, so that the center-of-mass oscillates indefinitely at the plasma frequency without any damping (Kohn mode). In this case, it was observed in previous simulations [14, 15] that the quantum fidelity never decays. To trigger sufficiently strong anharmonic effects, we take $x_0 = 3\sigma_x$ and $K = 0.1\sigma_x^2$ (K has the dimensions of an inverse square length). The parameters K and x_0 will take these values for all the forthcoming simulations, whereas η and H will be varied to study their impact on the quantum fidelity.

3.1. General results on the fidelity decay

The typical behavior of the quantum fidelity (figure 1) shows the same pattern already observed in the previous studies of interacting many-particle systems [14, 15]; after a quiescent period, the fidelity drops abruptly to very small values. Notice that, because of numerical dissipation, the standard fidelity F slightly decreases during the initial phase, but this artefact is removed when using the renormalized fidelity F_{W}.

Next, we plot the critical time (i.e. the time at which the fidelity starts dropping) versus the initial perturbation δv_0 (figure 2). The critical time is defined as the time at which the fidelity has dropped to 98% of its maximum value, i.e. $F_{\mathrm{W}}(\tau_{\mathrm{C}}) = 0.98$. (In the previous studies, we had used smaller values, e.g. 60% or 80%. However, as will become clear from the forthcoming analysis, the relevant quantity is the time at which the fidelity starts dropping.) It is evident from the figure that the logarithmic dependence observed in previous studies is recovered for the Wigner–Poisson model used here, i.e.

$$\tau_{\mathrm{C}} = -\tau_0 \ln \delta v_0 + \mathrm{const.} \tag{7}$$

Both the slope τ_0 and the additive constant depend on the value of the filling fraction η.

The above behavior was not entirely elucidated in [14, 15]. It could be established that the sudden drop of the fidelity occurs on a timescale that is close to the oscillation period T of

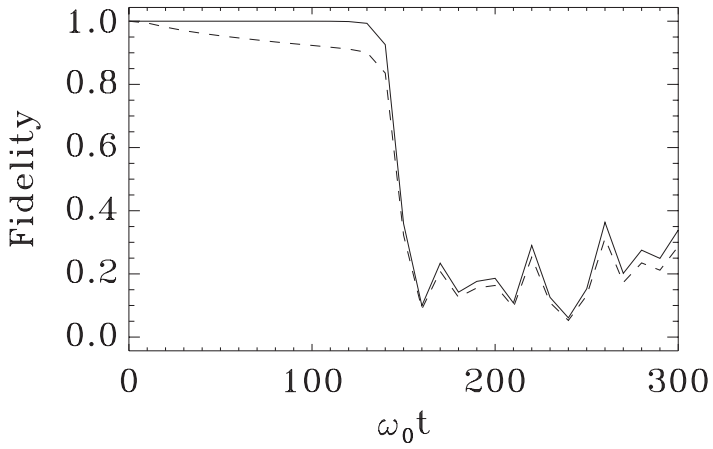

Figure 1. Typical behavior of the quantum fidelity for $\eta = 6$, $H = 1$ and $\delta v_0 = 10^{-8} v_{\rm th}$. The dashed line represents the standard fidelity (equation (5)), whereas the solid line corresponds to the renormalized fidelity (equation (6)).

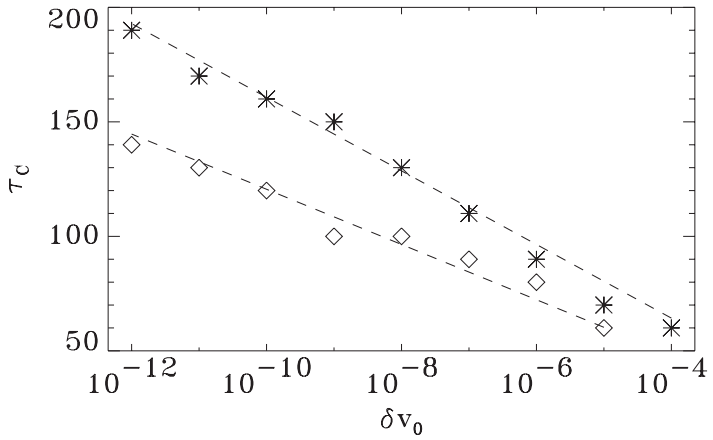

Figure 2. Critical time $\tau_{\rm C}$ (in units of ω_0^{-1}) versus perturbation amplitude δv_0 (in units of $v_{\rm th}$), for $H = 1$ and $\eta = 6$ (stars) and $\eta = 8$ (diamonds). The straight-dashed lines are theoretical estimates based on equation (8).

a classical particle evolving in the confining potential. Here, $\omega_0 T \simeq 4.2$ which is compatible with figure 1 (note that the fidelity is sampled at intervals of $10\omega_0^{-1}$). The slope and the additive constant appearing in equation (7) are more problematic. In the following, we present some theoretical considerations that allow us to provide a full quantitative picture of the origin of this anomalous behavior.

The logarithmic dependence can be interpreted in terms of trajectory separations. This is one reason why the approach adopted here—i.e. perturbing the initial state rather than the Hamiltonian—is particularly attractive. We are interested in the evolution of the mean velocity: $\langle v_i(t)\rangle = \iint f_i(x, v, t) v \, {\rm d}x \, {\rm d}v$, $i = 1, 2$ (the same line of reasoning could be followed for the average position $\langle x_i\rangle$). The separation between evolution one and evolution two can be quantified by the distance between the respective mean velocities: $\delta v(t) = \langle v_1(t)\rangle - \langle v_2(t)\rangle$. Obviously $\delta v(t = 0) = \delta v_0$.

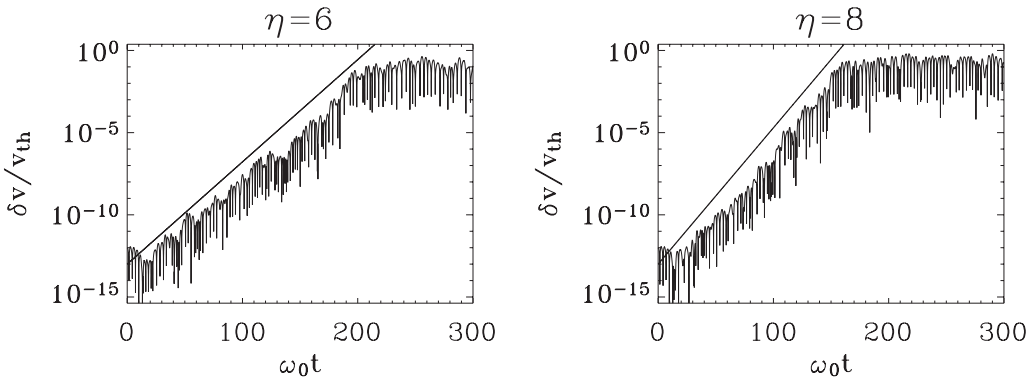

Figure 3. Separation of the mean velocities $\delta v(t)$ versus time, for $H = 1$ and initial perturbation $\delta v_0 = 10^{-12} v_{\rm th}$. Left panel: $\eta = 6$; right panel: $\eta = 8$. The straight lines are exponentials with growth rates $\lambda = 0.9 T_0^{-1}$ for $\eta = 6$ and $\lambda = 1.2 T_0^{-1}$ for $\eta = 8$.

Now, let us suppose that the initial perturbation δv_0 increases exponentially: $\delta v(t) = \delta v_0 \exp(\lambda t)$, where λ is a kind of 'Lyapunov exponent'. Inverted commas are in order, because the Lyapunov exponents are normally defined for single classical trajectories, whereas here we consider the evolution of averaged quantities computed from a quantum phase-space distribution. Nevertheless, some authors have considered this problem previously [21, 22]. We make the hypothesis that the critical time $\tau_{\rm C}$ occurs when the separation between the two evolutions reaches a critical value $\delta v_{\rm C}$, which yields $\tau_{\rm C} = -\lambda^{-1}(\ln \delta v_0 - \ln \delta v_{\rm C})$. The critical value corresponds to a perturbation that is quantum-mechanically large. This can be estimated as $\delta v_{\rm C} \simeq \hbar / m_* \sigma_x = H v_{\rm th}$. Using this value, we obtain finally

$$\tau_{\rm C} = -\frac{1}{\lambda}\left[\ln\left(\frac{\delta v_0}{v_{\rm th}}\right) - \ln H\right]. \tag{8}$$

Within this interpretation, $\tau_{\rm C}$ constitutes a sort of Ehrenfest time for our system.

Equation (8) makes a definite prediction on both the slope and the additive constant of the curves in figure 2. In particular, the slope should be given by the inverse of the Lyapunov exponent λ. To check this conjecture, in figure 3, we plot the distance $\delta v(t)$ between the mean velocities, for the two cases with $\eta = 6$ and $\eta = 8$. It is clear that δv grows exponentially in accordance with our conjecture. The computed growth rates (Lyapunov exponents) are $\lambda = 0.9 T_0^{-1}$ for $\eta = 6$ and $\lambda = 1.2 T_0^{-1}$ for $\eta = 8$. Here, $T_0 = 2\pi/\omega_0$ is the classical linear period of oscillation in the confining potential. Now, these values correspond neatly to the slopes of the straight lines depicted in figure 2. In addition, the measured Lyapunov exponents do not depend on the initial perturbation δv_0.

The additive constant in equation (8) depends on $\hbar$. To test the accuracy of this formula, we have performed additional simulations with a smaller normalized Planck constant, $H = 0.2$. The results are shown in figure 4. Again, we observe a logarithmic dependence of the critical time with the initial perturbation. We have checked that the observed slope τ_0 is indeed equal to the inverse of the Lyapunov exponent λ. The two straight lines in figure 4 are the theoretical estimates based on equation (8): the solid line corresponds to the actual value $H = 0.2$ and the dashed line to $H = 1$. Even though the difference is small, because the dependence on H is logarithmic, it is clear that the solid line provides a better fit to the numerical data, thus confirming the accuracy of equation (8).

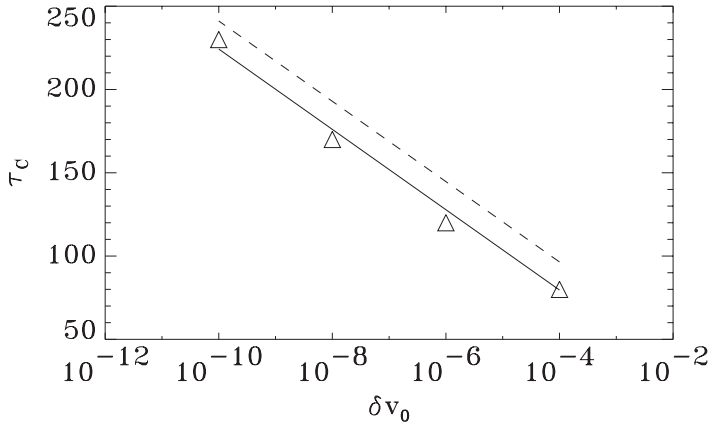

Figure 4. Critical time τ_C (in units of ω_0^{-1}) versus perturbation amplitude δv_0 (in units of v_{th}), for $H = 0.2$ and $\eta = 6$ (triangles). The straight lines are theoretical estimates based on equation (8): the solid line corresponds to $H = 0.2$ and the dashed line to $H = 1$.

Thus, equation (8) provides all the elements to compute the critical time *for any value of the initial perturbation* δv_0, provided the normalized Planck constant H and the Lyapunov exponent λ are known. The latter can be computed from a single simulation for an arbitrary (though sufficiently small) value of δv_0.

The above considerations also explain why no fidelity drop is observed for purely harmonic confinement ($K = 0$). In this case, Kohn's theorem [8] states that the average velocity $\langle v \rangle$ simply oscillates at the frequency ω_0, irrespective of the internal self-consistent dynamics. Thus, $\delta v(t)$ stays equal to its initial value at all times, and can never reach the critical value δv_C.

It must be noted that a similar behavior was observed for the linear Schrödinger equation (single-particle dynamics) in a given chaotic Hamiltonian [23, 24]. In that case, the fidelity stayed equal to unity until a critical time, after which it started to decay exponentially. An interpretation in terms of the Ehrenfest time was also provided in [24]. However, no sudden drop was observed after the critical time, as is the case for our simulations.

In view of the above considerations, we can conclude that:

- The quiescent period during which the fidelity stays equal to unity does not arise from self-consistent effects. It appears whenever the initial perturbation is small compared to $\hbar$ [24], i.e. in the present notation, $\delta v_0 / v_{th} \ll H$.
- The rapid drop of the fidelity after τ_C is a self-consistent effect. It is not seen in simulations of the linear Schrödinger equation, where, in contrast, an exponential decay is always observed after the initial quiescent period. Physically, this is related to the fact that the Hamiltonian depends on the electron density through the Poisson's equation (2). When the two evolutions start diverging, the Hamiltonian is itself modified, which in turn affects electron density, and so on. Because of this nonlinear loop, the two evolutions can diverge very fast (i.e. on the timescale of the plasma frequency or the frequency of the external confinement). In contrast, for the linear single-particle dynamics, the Hamiltonian is fixed and the solutions only diverge because of the small perturbation. Changes add incrementally to each other, but cannot trigger the nonlinear loop observed in the self-consistent simulations.

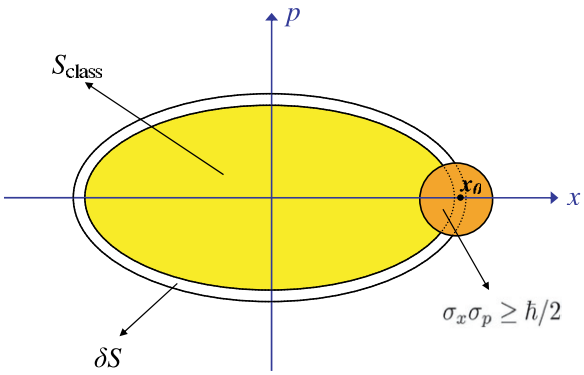

Figure 5. Schematic representation of the various action quantities involved in the problem. For the meaning of the symbols, see the main text.

One may wonder why, for the self-consistent systems studied here and in our previous works, we were always in a situation where the initial perturbation was small compared to $\hbar$. To understand this let us identify the various actions that are involved in the present problem (see figure 5). They are: (i) the typical classical action S_{class}, given by the area of phase space included in a classical orbit with initial condition $x(0) = x_0$, $v(0) = 0$; (ii) the perturbation δS, proportional to δv_0; (iii) the extension of the initial state in phase space $\sigma_x\sigma_p$; and finally (iv) the Planck's constant $\hbar$. Two conditions must always be satisfied: $\sigma_x\sigma_p \geqslant \hbar/2$ (the uncertainty principle) and $\delta S \ll S_{\text{class}}$ (because the perturbation must be classically small by definition). Thus, the scaling used in the present and previous works of ours is the following:

$$S_{\text{class}} > \sigma_x\sigma_p \geqslant \hbar/2 \gg \delta S. \tag{9}$$

In practice, this is a realistic scaling for electronic systems operating in a quantum regime (i.e. $\sigma_x\sigma_p \approx \hbar$), such as quantum dots and quantum wells.

In contrast, when the perturbation δS is of the same order of magnitude as the Planck's constant, two other regimes can be envisaged. The first is a quantum regime where

$$S_{\text{class}} > \sigma_x\sigma_p \approx \delta S \approx \hbar/2. \tag{10}$$

In this case $\delta v_0 \approx \delta v_{\text{C}}$, so that the quiescent period shrinks to zero and the fidelity drops at the very beginning of the simulation.

The second regime is characterized by the scaling

$$S_{\text{class}} > \sigma_x\sigma_p \gg \delta S \approx \hbar/2. \tag{11}$$

This is a semiclassical regime ($H \ll 1$) where the perturbation is classically small but quantum-mechanically large, as in the original study by Jalabert and Pastawski [11]. Thus, one might expect to recover an exponential decay at the classical Lyapunov or Fermi golden rule rate. However, this regime is very hard to attain in numerical simulations of the Wigner equation, because of the formation of small-scale structures in the phase space. In the next subsection, we will explore the impact of the normalized Planck constant H, and hence of the electron temperature on the fidelity decay. Nevertheless, the initial perturbation will be kept small, so that we still operate in the regime given by equation (9).

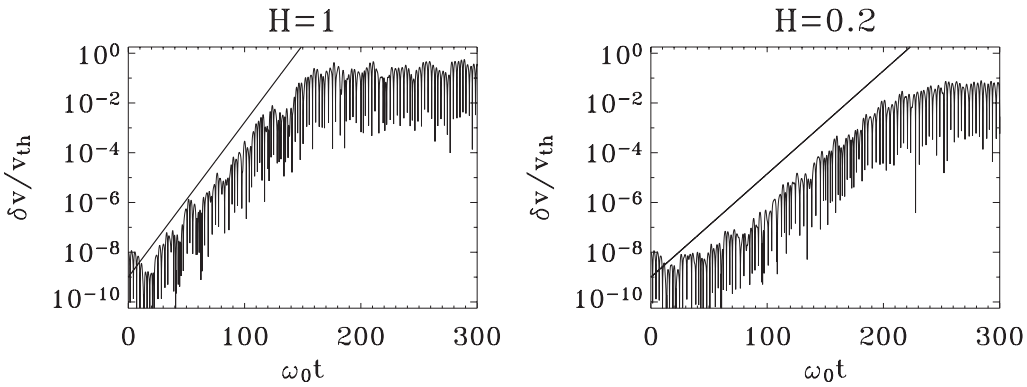

Figure 6. Separation of the mean velocities $\delta v(t)$ versus time, for $\eta = 6$ and initial perturbation $\delta v_0 = 10^{-8} v_{\rm th}$. Left panel: $H = 1$; right panel: $H = 0.2$. The straight lines are exponentials with growth rates $\lambda = 0.9 T_0^{-1}$ for $H = 1$ and $\lambda = 0.6 T_0^{-1}$ for $H = 0.2$.

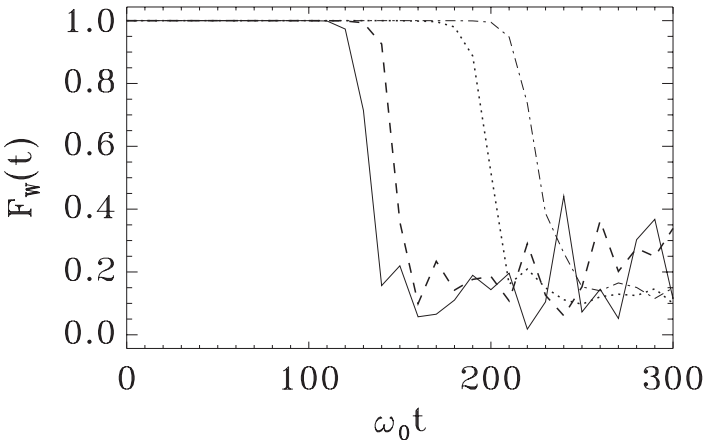

Figure 7. Quantum fidelity $F_{\rm W}$ for $\eta = 6$, $\delta v_0 = 10^{-8} v_{\rm th}$, and various values of Planck's constant: $H = 2$ (solid line), $H = 1$ (dashed line), $H = 0.2$ (dotted line), and $H = 0.1$ (dot-dashed line).

3.2. Effect of Planck's constant

As is apparent from equation (8), the critical time $\tau_{\rm C}$ depends logarithmically on the normalized Planck constant H. Physically, this is because the initial perturbation δv_0 saturates at a value $\delta v_{\rm C}$ that is proportional to H. However, for self-consistent problems, the Hamiltonian is itself a function of the Planck constant, and therefore we also expect the Lyapunov exponent λ to depend on H.

Figure 6 shows the trajectory separation $\delta v(t)$ for two values of H. Here, the effect of H is very clear. On one hand, $\delta v(t)$ saturates at a lower level for smaller H, because of the $\ln H$ dependence in equation (8). This effect would tend to reduce $\tau_{\rm C}$ with decreasing H. On the other hand, we see that the Lyapunov exponent λ decreases with H, which tends to increase $\tau_{\rm C}$ with decreasing H. The latter effect is stronger, so that the critical time increases with decreasing Planck constant, as can be seen from figure 7.

The above results should be considered with some caution. As was mentioned earlier, the numerical dissipation is stronger in the semiclassical limit. This can be measured by the entropy-like quantity $\iint f^2\,\mathrm{d}x\,\mathrm{d}v$, which decreases monotonically with time. In the above runs with $0.1 \leqslant H \leqslant 2$, the numerical resolution was chosen so that $\iint f^2\,\mathrm{d}x\,\mathrm{d}v$ never falls below 80% of its initial value, which should guarantee enough accuracy. Nevertheless, one cannot completely rule out some numerical effect on the measured values of τ_{C} and λ.

3.3. Effect of decoherence

One of the toughest challenges for the construction of an actual quantum computer is the omnipresence of decoherence. Decoherence occurs when a quantum system, initially in a pure state, deteriorates into a quantum mixture because of its coupling to a complex environment. Crucial quantum features such as entanglement are lost in this process, which reduces dramatically the computing efficiency.

It is therefore interesting to study the influence of an external environment on the decay of the quantum fidelity. In solid-state devices, decoherence is typically due to disorder or phonon scattering. This can be modeled [25] in the form of a friction–diffusion term on the right-hand side of the Wigner equation (1):

$$\left(\frac{\partial f}{\partial t}\right)_{\mathrm{scatt}} = 2\gamma\frac{\partial (vf)}{\partial v} + D_v\frac{\partial^2 f}{\partial v^2} + D_x\frac{\partial^2 f}{\partial x^2}, \tag{12}$$

where γ is the relaxation rate and D_v, D_x the diffusion coefficients in velocity and real space respectively, which are related to the decoherence time. In order for equation (1) to preserve the positivity of the density matrix associated to the Wigner distribution function, the scattering term must be in Lindblad form. This is automatically achieved [26] if the above coefficients respect the inequality $D_v D_x \geqslant \gamma^2\hbar^2/4m_*^2$. In general, we shall take the equality sign in the preceding relation. The diffusion coefficient in velocity space is taken to be $D_v = \gamma v_{\mathrm{th}}^2$. Thus, only the relaxation rate γ remains to be specified.

To study the effect of decoherence, we begin our simulations with a pure quantum state, which corresponds to $H = 2$. Due to the dissipative terms, the initially pure state deteriorates into a quantum mixture. The degree of 'purity' can be measured by the quantity

$$\Sigma(t) = \frac{2\pi\hbar}{m_* N^2}\iint f^2\,\mathrm{d}x\,\mathrm{d}v, \tag{13}$$

($N = \iint f\,\mathrm{d}x\,\mathrm{d}v$), which satisfies $0 \leqslant \Sigma \leqslant 1$ for a mixed-quantum state and $\Sigma = 1$ for a pure state [18, 27].

The evolution of the purity, shown in figure 8, is identical irrespective of the initial perturbation, i.e. $\iint f_1^2\,\mathrm{d}x\,\mathrm{d}v = \iint f_2^2\,\mathrm{d}x\,\mathrm{d}v$ for all times. The environment-induced decoherence time τ_{D} can be estimated by fitting the purity curves with a decaying exponential. By doing so, we obtain $\omega_0\tau_{\mathrm{D}} = 234$, 142 and 58, for $\gamma/\omega_0 = 10^{-4}$, 2×10^{-4}, and 5×10^{-4}, respectively. Notice that the purity curves tend to reach asymptotically the same value, irrespective of their decay rate. This saturation corresponds to the spreading of the Wigner function over all the accessible phase space (i.e. the classical action S_{class}).

The effect of decoherence is to smooth out small-scale oscillations in the phase space structure of the Wigner function. These oscillations represent typically the quantum correlations. As a standard example, let us consider a wavefunction made of the superposition of two Gaussians centered at $x = \pm d/2$. Its Wigner transform is given by two phase-space Gaussians

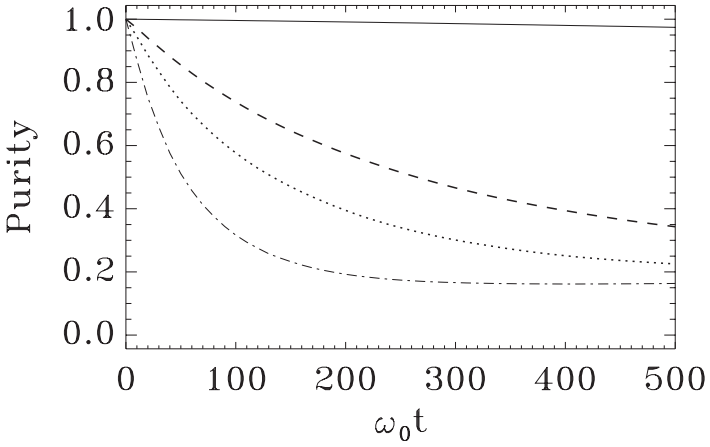

Figure 8. Evolution of the purity for $\eta = 6$, $H = 2$ and $\delta v_0 = 10^{-8} v_{\rm th}$. The relaxation rate (in units of ω_0) is $\gamma = 0$ (solid line), $\gamma = 10^{-4}$ (dashed line), $\gamma = 2 \times 10^{-4}$ (dotted line) and $\gamma = 5 \times 10^{-4}$ (dot-dashed line).

centered at $p = 0$ and $x = \pm d/2$, plus oscillating terms appearing half-way between the two Gaussians and with a velocity-space wavenumber $k_v = dm_*/\hbar$.

A diffusive term such as that appearing in equation (12) destroys the velocity–space structures with wavenumber k_v in a typical time $\tau_{\rm D} = (D_v k_v^2)^{-1}$. Since $D_v = \gamma v_{\rm th}^2$, we obtain that $\gamma \tau_{\rm D} = (k_v v_{\rm th})^{-2}$. From the computed values of the coherence time, we notice that the product $\gamma \tau_{\rm D}$ is about the same for all values of γ, and it equals roughly 0.027. This means that, in all cases, the oscillating structure of the Wigner function is concentrated near a single velocity-space wavenumber $k_v = (\gamma \tau_{\rm D})^{-1/2} v_{\rm th}^{-1}$. This yields a typical velocity-space wavelength $\lambda_v = 2\pi/k_v = 2\pi (\gamma \tau_{\rm D})^{1/2} v_{\rm th} \simeq 1.03 v_{\rm th}$.

The above estimate can be checked directly by looking at the phase-space portrait of the Wigner function, shown in figure 9. In this case, $\gamma = 2 \times 10^{-4} \omega_0$ and the decoherence time is $\omega_0 \tau_{\rm D} = 142$. For $\omega_0 t = 60$ (i.e. shorter than $\tau_{\rm D}$) a fine interference pattern is present in the phase space. The typical velocity wavelength can be extracted from a cross-cut of the Wigner function at $x = 0$ (bottom frames of the figure), and it appears to be in good agreement with the above estimation. The interesting point is that measuring the decoherence time from the evolution of the purity (i.e. a global measure) allowed us to estimate the typical size of velocity-space structures without actually looking at the Wigner function itself.

On the other hand, the interference pattern is destroyed for times much larger than the decoherence time (see plots for $\omega_0 t = 700$ in figure 9) and the resulting phase-space distribution is smooth. In this case, the Wigner function is also everywhere positive: the quantum correlations have leaked out into the environment and the Wigner function can now be safely interpreted as a classical probability density.

We now turn our attention to the evolution of the quantum fidelity. In the previous sections, the normalized fidelity $F_{\rm W}$ was used to remove the artefact arising from a small numerical dissipation, as was shown in figure 1. Here, however, the dissipation is a real effect due to the presence of a finite relaxation rate γ. Therefore, it is better to revert to the original definition of the quantum fidelity (equation (5)), which is shown in figure 10 for different values of γ. It is clear that the fidelity decreases in two different manners: (i) a continuous, roughly exponential

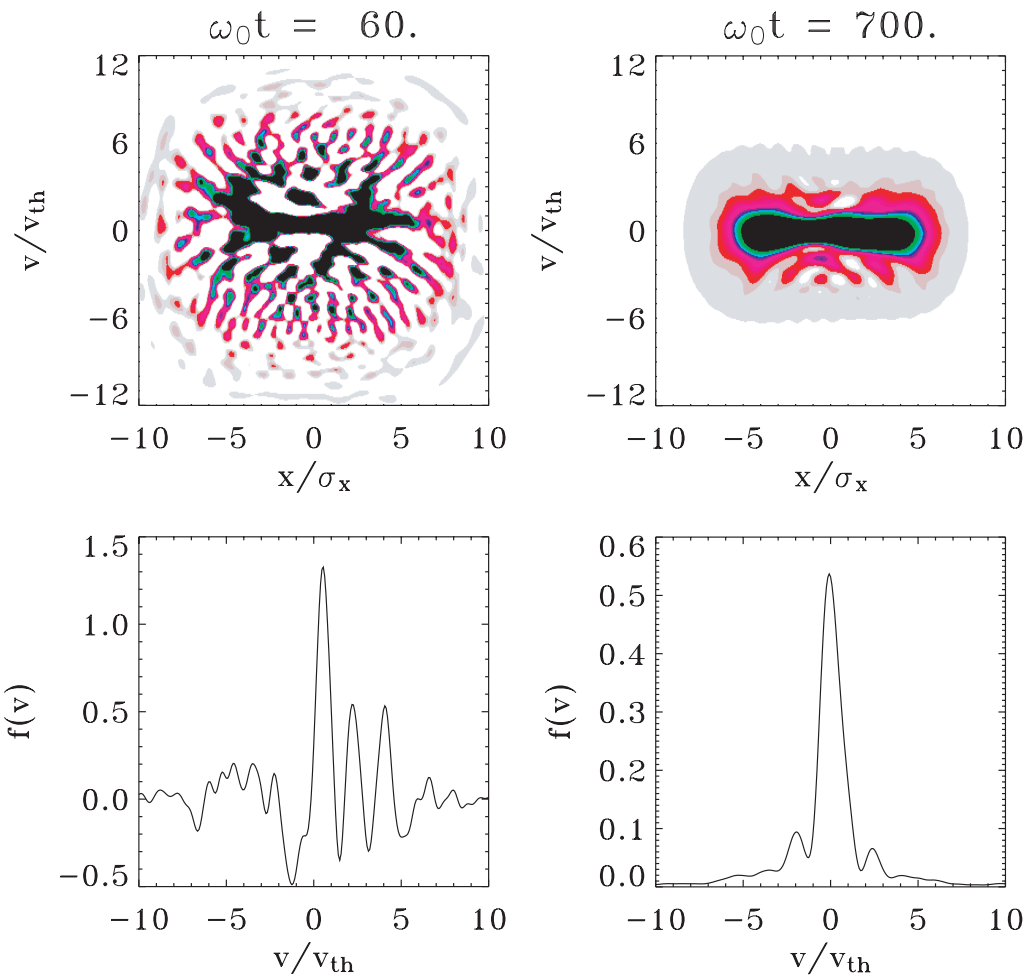

Figure 9. Phase space portraits of the Wigner function for $\gamma = 2 \times 10^{-4}\omega_0$, at times $\omega_0 t = 60$ (left panels) and $\omega_0 t = 700$ (right panels). The bottom panels show a cross-cut of the Wigner function at $x = 0$. Here, $H = 2$ and $\eta = 6$.

decay over a timescale τ_D due to the environmental decoherence and (ii) a sudden drop at τ_C, which reflects the instability of the systems under small perturbations of the initial condition. The first mechanism is dissipative, whereas the second is unitary. Nevertheless, both represent a sort of effective decoherence for the system under study. It seems appropriate to term the first mechanism 'environment-induced decoherence' (occurring on a timescale τ_D) and the second 'internal decoherence' (timescale equal to τ_C). Depending on the value of τ_D and τ_C, either mechanism will dominate in a specific situation. In particular, the sudden fidelity drop is suppressed when τ_D becomes smaller than τ_C. Both mechanisms involve the formation of subtle quantum correlations (represented by small scale structures in the phase space). In the case of environment-induced decoherence, these correlations trickle out into the environment and are lost forever from the point of view of the system. In the case of internal decoherence, the correlations are transferred from the center-of-mass to the relative coordinates. They are still present in the electron system but become increasingly difficult to track down in practice, because a minimal error in the initial condition eventually leads to very different evolutions.

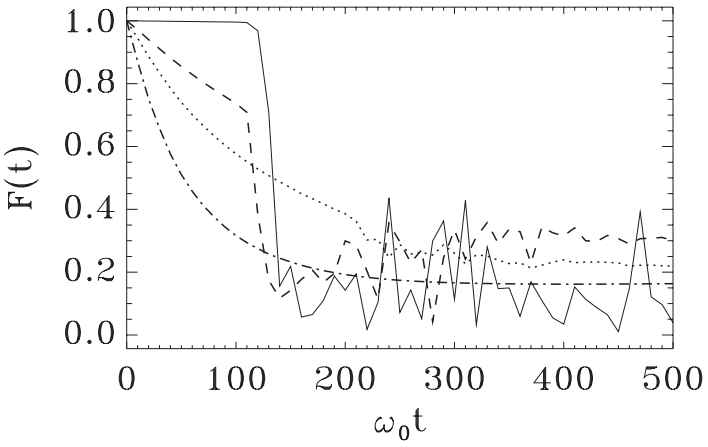

Figure 10. Evolution of the quantum fidelity $F(t)$ for $\eta = 6$, $H = 2$ and $\delta v_0 = 10^{-8} v_{\rm th}$. The relaxation rate (in units of ω_0) is $\gamma = 0$ (solid line), $\gamma = 10^{-4}$ (dashed line), $\gamma = 2 \times 10^{-4}$ (dotted line) and $\gamma = 5 \times 10^{-4}$ (dot-dashed line).

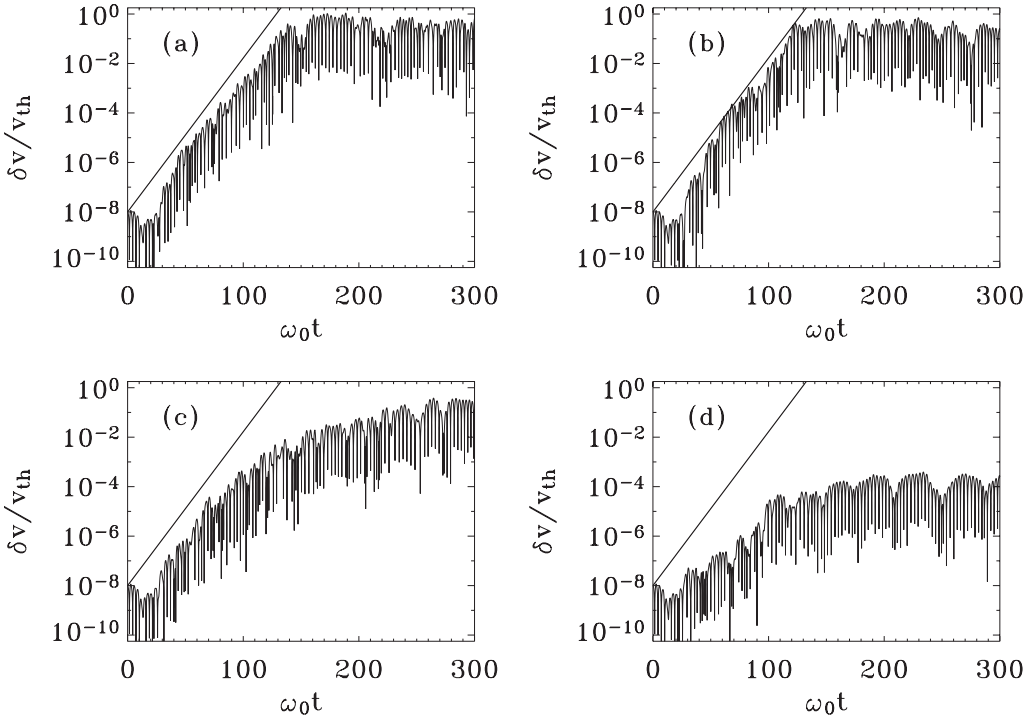

Figure 11. Separation of the mean velocities $\delta v(t)$ versus time, for $H = 2$, $\eta = 6$ and initial perturbation $\delta v_0 = 10^{-8} v_{\rm th}$. (a) $\gamma = 0$, (b) $\gamma = 10^{-4}$, (c) $\gamma = 2 \times 10^{-4}$ and (d) $\gamma = 5 \times 10^{-4}$ (in units of ω_0). The straight lines are exponentials with growth rate $\lambda = 0.9 T_0^{-1}$.

For harmonically confined systems the center-of-mass and relative coordinates are decoupled so that no internal decoherence can be observed.

Finally, figure 11 shows the evolution of $\delta v(t)$ for various values of the relaxation rate, from $\gamma = 0$ to $\gamma = 5 \times 10^{-4} \omega_0$. The latter value corresponds to a relaxation time $\gamma^{-1} \approx 330$ ps. As

long as $\gamma < 10^{-4}\omega_0$, no effect is noticed on the trajectory separation. Around $\gamma = 2 \times 10^{-4}\omega_0$, the Lyapunov exponent starts decreasing, so that the echo is reached for longer times (see the corresponding fidelity curve in figure 10, where the echo is visible as a small kink at $\omega_0 t \simeq 200$). For even larger values of γ, δv saturates at a much lower level, smaller than the critical value δv_C. In this case, the Loschmidt echo cannot occur in accordance with what was observed in figure 10 for $\gamma = 5 \times 10^{-4}\omega_0$.

4. Conclusion

In this paper, we have investigated the self-consistent dynamics of the electron gas confined in a nonparabolic quantum well. Compared to the previous studies on the Loschmidt echo in systems of interacting particles, several novel aspects were analyzed here: (i) the dynamics was described by the Wigner–Poisson system, which can deal with both pure and mixed quantum states; (ii) as the Wigner–Poisson system is nonlinear, it was possible to perturb the initial condition rather than the Hamiltonian; (iii) the dependence on the effective Planck constant was investigated; and finally (iv) the effect of the decoherence induced by an external environment was analyzed.

As in the previous studies on interacting systems, it was found that the quantum fidelity remains constant until a certain critical time, after which it drops suddenly, typically on the timescale of the confining trap. A comprehensive argument—in terms of the system's Ehrenfest time—was put forward to explain this behavior. Comparison with numerical results yielded very good agreement.

It was also found that the environment-induced decoherence can suppress the Loschmidt echo efficiently, by smoothing the distribution function over a phase-space region $\sim\hbar$ before the echo has had time to occur. Indeed, the Loschmidt echo and the environmental decoherence are competing effects that both tend to reduce the quantum fidelity. We have referred to these two phenomena as 'environment-induced' and 'internal' decoherence, each characterized by its own timescale. The existence of a finite internal decoherence suggests that even in the absence of coupling to an external environment a many-body quantum system might not, in practice, be perfectly reversible.

Our findings thus clarify the anomalous behavior of the quantum fidelity observed in the numerical simulations of interacting systems so far studied [14, 15]. They may help in quantifying the stability and coherence properties of solid-state devices that are envisaged for the practical implementation of quantum computers.

Finally, it must be stressed that both the present results and those of [14, 15] were obtained in the context of dynamical mean-field models. Indeed, the Wigner–Poisson system used here is equivalent to the time-dependent Hartree equations. A natural further step along this line of research would lead us to investigate the *exact* electron dynamics, perhaps in the simpler case of two or three electrons [28], which would be highly relevant to current laboratory experiments [29]. An exact study of the few-electron dynamics would nicely complement and extend the present mean-field many-electron results.

References

[1] Loss D and DiVincenzo D P 1998 *Phys. Rev.* A **57** 120
[2] Zoller P *et al* 2005 *Eur. Phys. J.* D **36** 203
[3] Gorman J, Hasko D G and Williams D A 2005 *Phys. Rev. Lett.* **95** 090502

[4] Jönsson L, Steiner M M and Wilkins J W 1997 *Appl. Phys. Lett.* **70** 1140
[5] Müller T, Parz W, Strasser G and Unterrainer K 2004 *Phys. Rev.* B **70** 155324
Pereira M F and Wenzel H 2004 *Phys. Rev.* B **70** 205331
[6] Nikonov D E, Imamoglu A, Butov L V and Schmidt H 1997 *Phys. Rev. Lett.* **79** 4633
[7] Wijewardane H O and Ullrich C A 2004 *Appl. Phys. Lett.* **84** 3984
[8] Kohn W 1961 *Phys. Rev.* **123** 1242
[9] Dobson J F 1994 *Phys. Rev. Lett.* **73** 2244
[10] Peres A 1984 *Phys. Rev.* A **30** 1610
[11] Jalabert R A and Pastawski H M 2001 *Phys. Rev. Lett.* **86** 2490
[12] Jacquod Ph, Silvestrov P G and Beenakker C W J 2001 *Phys. Rev.* E **64** 055203
[13] Cucchietti F M *et al* 2002 *Phys. Rev.* E **65** 046209
[14] Manfredi G and Hervieux P-A 2006 *Phys. Rev. Lett.* **97** 190404
[15] Manfredi G and Hervieux P-A 2008 *Phys. Rev. Lett.* **100** 050405
[16] Santer M, Mehlig B and Moseler M 2002 *Phys. Rev. Lett.* **89** 286801
[17] Gusev G M *et al* 2002 *Phys. Rev.* B **65** 205316
[18] Manfredi G and Feix M R 2000 *Phys. Rev.* E **62** 4665
[19] Manfredi G and Hervieux P-A 2007 *Appl. Phys. Lett.* **91** 061108
[20] Suh N, Feix M R and Bertrand P 1991 *J. Comput. Phys.* **94** 403
[21] Haake F, Wiedemann H and Zyczkowski K 1992 *Ann. Phys. Lpz.* **1** 531
[22] Ballentine L E 2001 *Phys. Rev.* A **63** 024101
[23] Benenti G and Casati G 2002 *Phys. Rev.* E **65** 066205
[24] Silvestrov P G, Tworzydlo J and Beenakker C W J 2003 *Phys. Rev.* E **67** 025204
[25] Zurek W H 2003 *Rev. Mod. Phys.* **75** 715
[26] Isar A, Sandulescu A, Scutaru H, Stefanescu E and Scheid W 1994 *Int. J. Mod. Phys.* E **3** 635
[27] Cucchietti F M, Dalvit D A R, Paz J P and Zurek W H 2003 *Phys. Rev. Lett.* **91** 210403
[28] Sako T, Hervieux P-A and Diercksen G H F 2006 *Phys. Rev.* B **74** 045329
[29] Kouwenhoven L, Oosterkamp T H, Danoesastro M W S, Eto M, Austing D G, Honda T and Tarucha S 1997 *Science* **278** 1788